

Strong Electronic Metal-Support Interaction Between Pt and Stainless Mesh for Enhancing Hydrogen Evolution Reaction

Jin Li,^a Jie Luo,^{‡b} Haipeng Chen,^a Bin Qin,^{*c} Changzhou Yuan,^{*d} Naiteng Wu,^{*a} Guilong Liu^a and Xianming Liu^{*a}

^aCollege of Chemistry and Chemical Engineering, and Henan Key Laboratory of Function-Oriented Porous Materials, Luoyang Normal University, Luoyang 471934, China

^bSchool of Chemical Engineering and Pharmaceutics, Henan University of Science and Technology, Luoyang 471023, China

^cDepartment of Chemistry, The University of Hong Kong, Pokfulam, Hong Kong SAR, China

^dSchool of Materials Science & Engineering, University of Jinan, Jinan, 250022 P. R. China

*Corresponding authors

‡ These authors contributed equally to this work

Experimental Section

All chemicals were analytical grade and were used without further purification. Prior to the synthesis, a piece of stainless mesh (SM, 304, 500 mesh) with a size of 1 cm × 3 cm was cleaned with ethanol and deionized water, respectively. The pretreated SM, 150 mg of hexadecyl trimethyl ammonium bromide (CTAB), and 50 mL of ethylene glycol were put in a 100 mL round-bottom flask, and maintained 150 °C in oil bath for 10 h with stirring. Afterwards, 50 μL of chloroplatinic acid (20 mg mL⁻¹) was quickly injected into the above solution with micro pipette, sequentially heated at 150 °C for 1h and then cooled down to room temperature. Finally, the as-synthesized sample was rinsed with ethanol and deionized water for several times, and naturally dried in air. The as-obtained product was named as Pt@SM and directly used for electrochemical measurements. In addition, the control experiments were also carried out without involving SM under the same operating condition. For comparison, the synthesized Pt nanoparticles on carbon cloth (Pt@CC) were developed with the same experimental condition.

Electrochemical measurements

All the electrochemical experiments were tested in an Argon-saturated 0.5 M H₂SO₄ (pH 0.28), 0.1M phosphate buffer (pH 7), and 1 M KOH (pH 14) solutions with a CHI660E electrochemical workstation (Chenhua, Co. Ltd., Shanghai). The as-synthesized electrode, carbon rod, and Hg/Hg₂Cl₂ electrode were used as the working electrode, counter electrode, and reference electrode, respectively. The measured potentials vs. Hg/Hg₂Cl₂ were calibrated to the reversible hydrogen electrode (RHE) scale according to the following Nernst equation: $E_{RHE} = E_{Hg/Hg_2Cl_2} + 0.0591pH + 0.244$. All the potentials reported in this work were manually 95% IR-corrected unless being specifically indicated. Before the electrochemical tests, the fresh-working electrode was activated and stabilized through repeating 100 times cyclic voltammetry (CV) with a scan of 100 mV s⁻¹, and the electrocatalytic performance of HER was evaluated by linear sweep voltammetry (LSV) at a scan rate of 2 mV s⁻¹. Tafel slope was acquired from LSV curves. Electrochemical impedance spectroscopy (EIS) measurements were carried out by using an AC voltage from 100 kHz to 0.01 Hz with an amplitude of 5 mV at -0.281 V. The Zview software was employed to fit the EIS results. To estimate the electrochemical active surface areas, CV was performed to assess the electrochemical double-layer capacitance (C_{dl}) under the potential window of 0.1-0.2 vs. RHE with different scan rates (100, 120, 140, 160, 180, and 200 mV s⁻¹). The current density differences ($\Delta j/2 = j_a/2 - j_c/2$, j_a and j_c are the anode and cathode current density, respectively) are plotted against scan rates, and the slopes can be used to derive the double-layer capacitance (C_{dl}). The stability of the catalyst was assessed through 10000 CV cycles between -0.2 and -0.5 V at a fixed scan rate of 50 mV s⁻¹. The chronopotentiometric measurement was performed at a constant current density of -100 mA cm⁻² for 45 h. For comparison, commercial 20% Pt/C powder or the as-synthesized Pt nanoparticles was dispersed in a mixed solution of 0.5 wt% Nafion and isopropanol, then sonicated to generate a homogeneous slurry. Finally, the as-obtained slurry containing Pt/C or Pt nanoparticles electrocatalyst was dropped onto the cleaned SM surface, resulting in an about Pt loading of 0.2 mg cm⁻². Gas generation was quantitatively performed by drainage method, and the cathodic electrolysis of Pt@SM was carried out at a constant current density of 50 mA cm⁻² for 60 min.

Materials Characterizations

The morphologies were analyzed by field emission scanning electron microscopy (FESEM, ZEISS-Merlin) and transmission electron microscopy (TEM, JEOL, JEM-2100F) equipped with the energy dispersive X-ray (EDX) mapping. X-ray diffraction (XRD) measurements were performed on a Bruker D8 advance setup. X-ray photoelectron spectroscopy (XPS) measurements were carried out on a Perkin-Elmer Model PHI 5600 XPS system with a resolution of 0.3-0.5 eV from a monochromatic aluminum anode X-ray source. Elemental analyses of catalyst samples were investigated by Inductively coupled plasma optical emission spectrometer (ICP-OES, Scientific iCAP 7600 Duo, ThermoFisher Scientific, Germany).

Computational calculations

The density functional theory (DFT) calculations were carried out by Vienna Ab-initio Simulation Package (VASP).¹⁻³ The generalized gradient approximation (GGA) of the Perdew-Burke-Ernzerhof (PBE) functional was employed to describe electron exchange and related effects.⁴⁻⁶ The pure Pt (111) and SM (111) slabs were both modeled with 15 Å vacuum and the K point was set up as 4 × 4 × 1, which were used for the geometric optimization of the catalyst surface. The cutoff energy for the plane-wave basis was set to 450 eV. Besides, the calculations were terminated until the maximum force upon each atom and energy were less than 0.05 eV/Å and 1.0 × 10⁻⁵ eV. The relevant Gibbs free energy change (ΔG_{H^*}) for adsorptions were calculated as: $\Delta G_{H^*} = E_{total} - E_{sur} - \frac{E_{H_2}}{2} + \Delta E_{ZPE} - T\Delta S$, where E_{total} is the total energy for the adsorption state, E_{sur} is the energy of pure surface, E_{H_2} is the total energy of H₂ gas, ΔE_{ZPE} is the zero-point energy change, T is the room temperature (298.15 K), and ΔS is the entropy change. Previous research has displayed that $\Delta E_{ZPE} - T\Delta S = 0.24$ eV, so ΔG_{H^*} can be defined as: $\Delta G_{H^*} = E_{total} - E_{sur} - \frac{E_{H_2}}{2} + 0.24$.

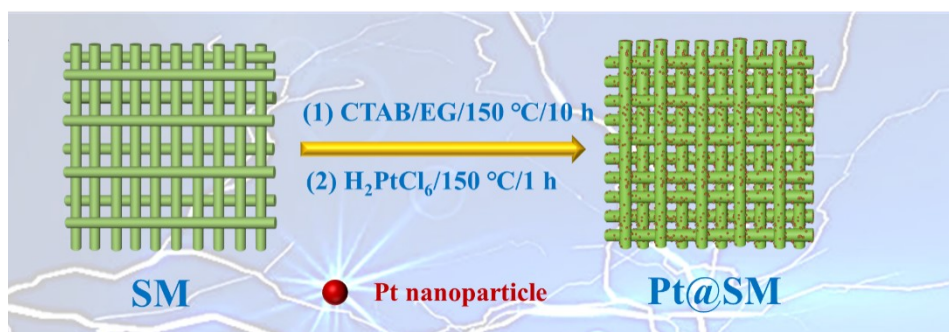


Fig. S1 Schematic illustration for the fabrication of Pt@SM.

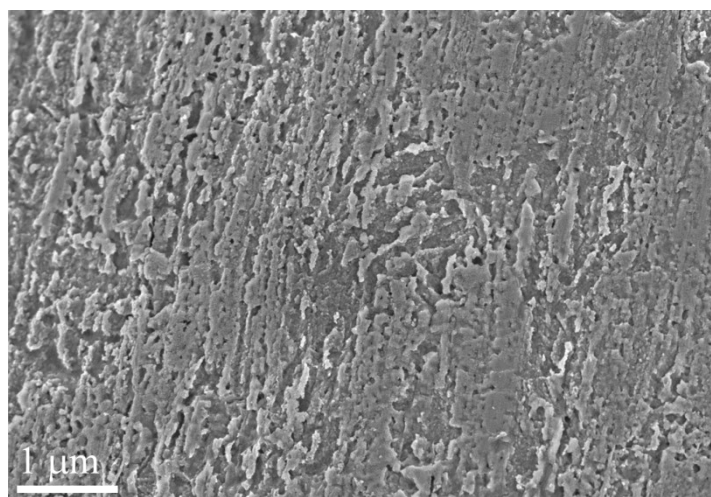


Fig. S2 FESEM of SM.

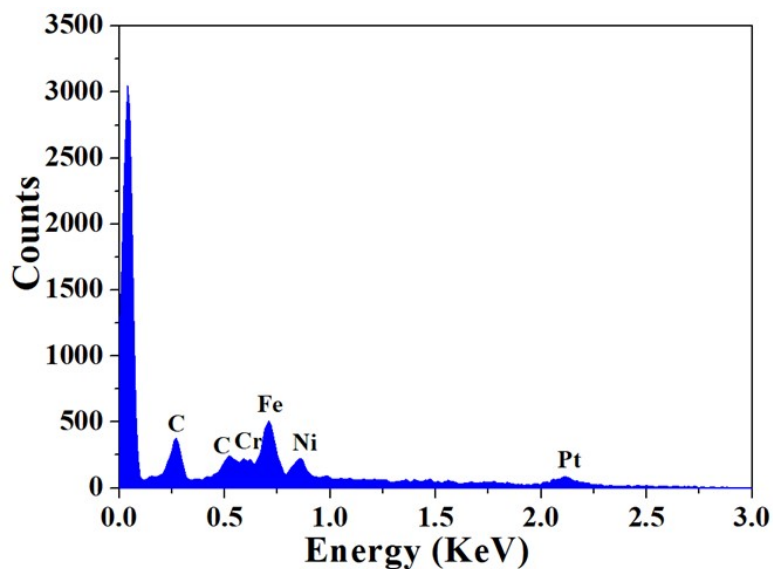


Fig. S3 EDX image of Pt@SM.

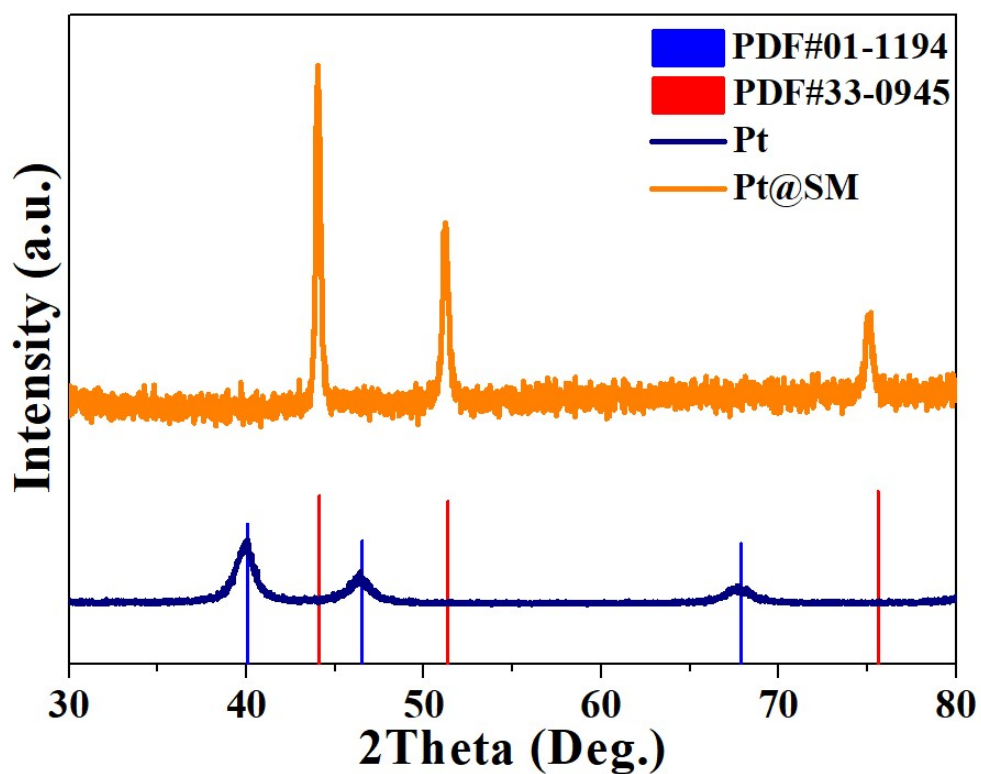


Fig. S4 XRD pattern of Pt@SM and Pt.

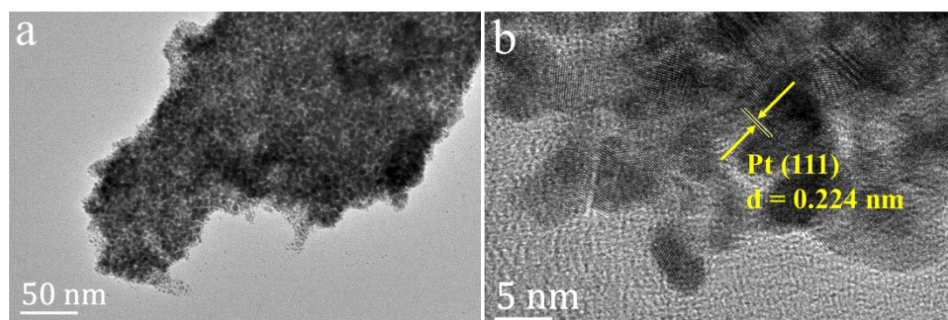


Fig. S5 TEM (a) and HRTEM (b) of Pt.

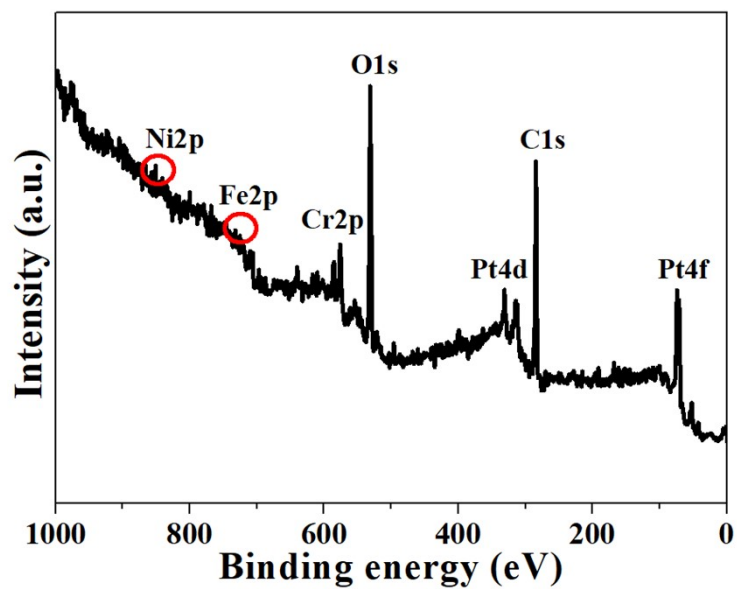


Fig. S6 XPS survey of Pt@SM.

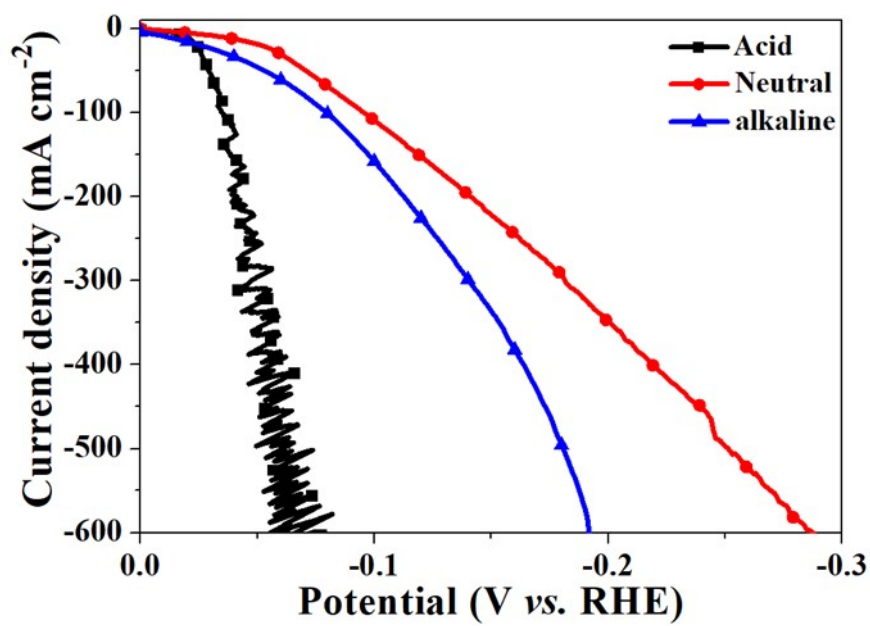


Fig. S7 LSV curves of Pt@SM at acid, neutral, and alkaline condition.

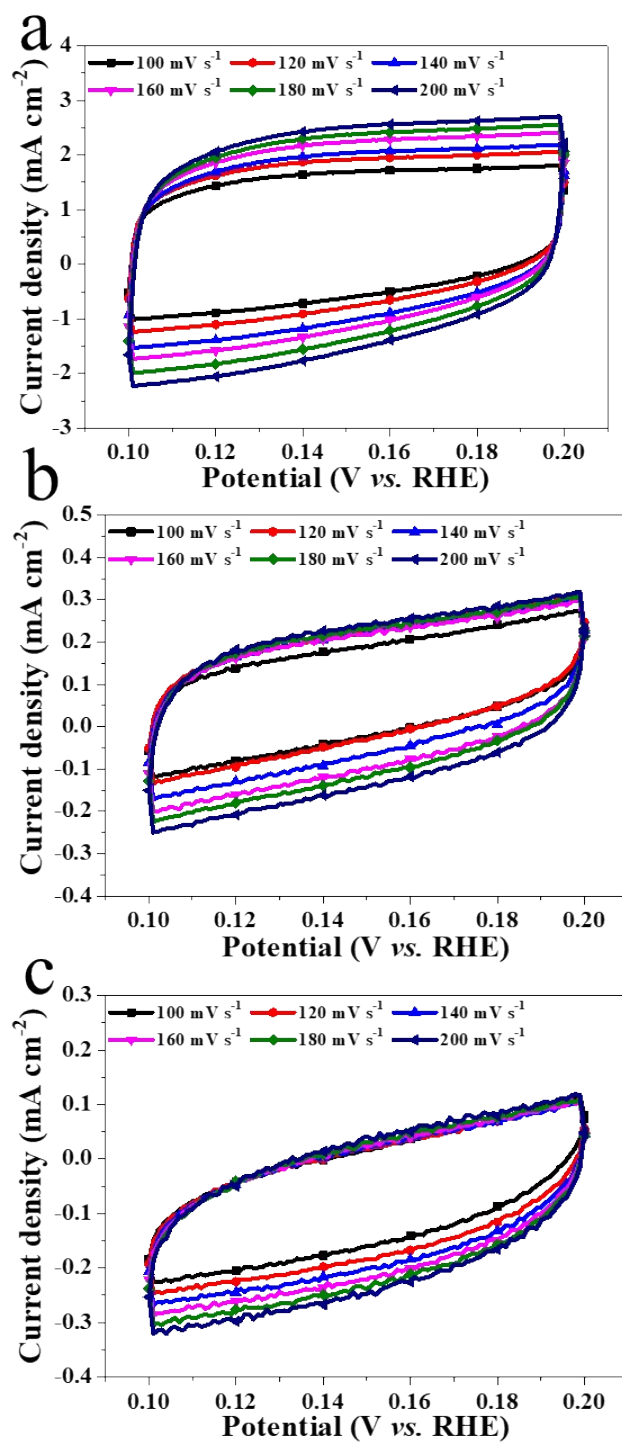


Fig. S8 Cyclic voltammograms of (a) Pt@SM, (b) Pt, and (c) SM samples in the non-faradaic capacitance current range at scan rates of 100, 120, 140, 160, 180, and 200 mV s⁻¹.

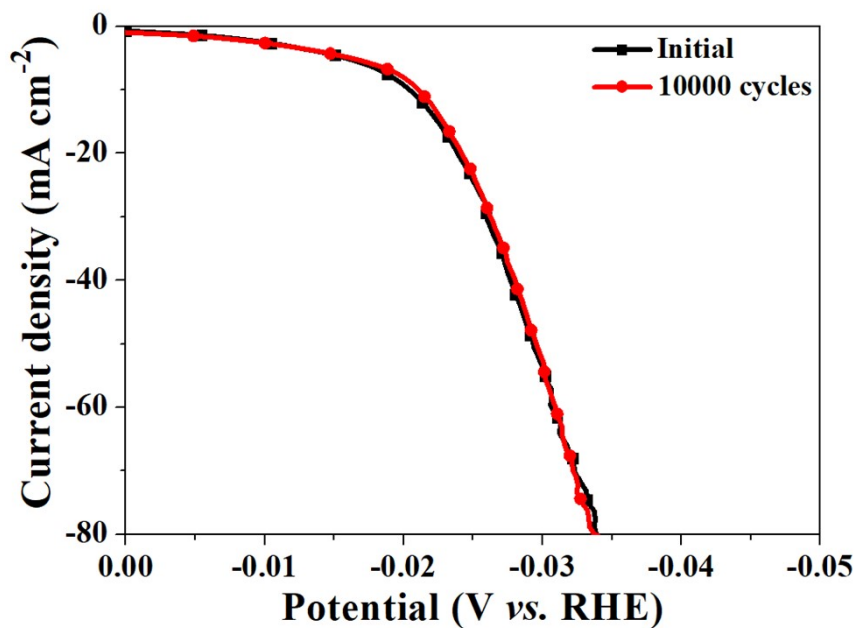


Fig. S9 LSV curves before and after 10000 cycles with IR compensation for Pt@SM.

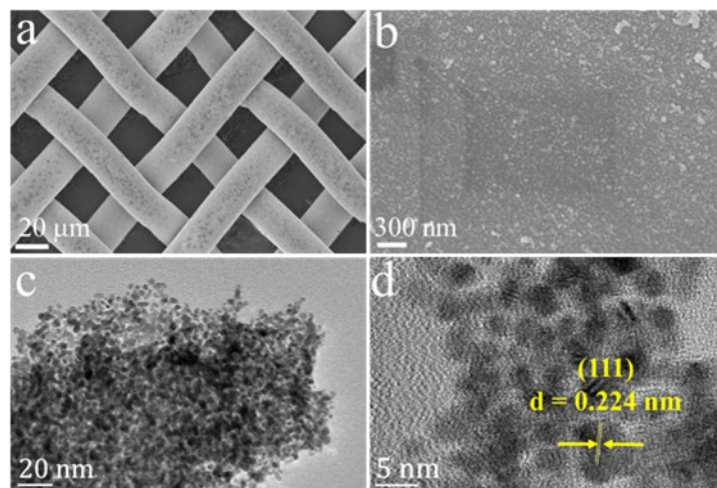


Fig. S10 (a,b) FESEM, (c) TEM, and (d) HRTEM images of Pt@SM after HER for 45 h.

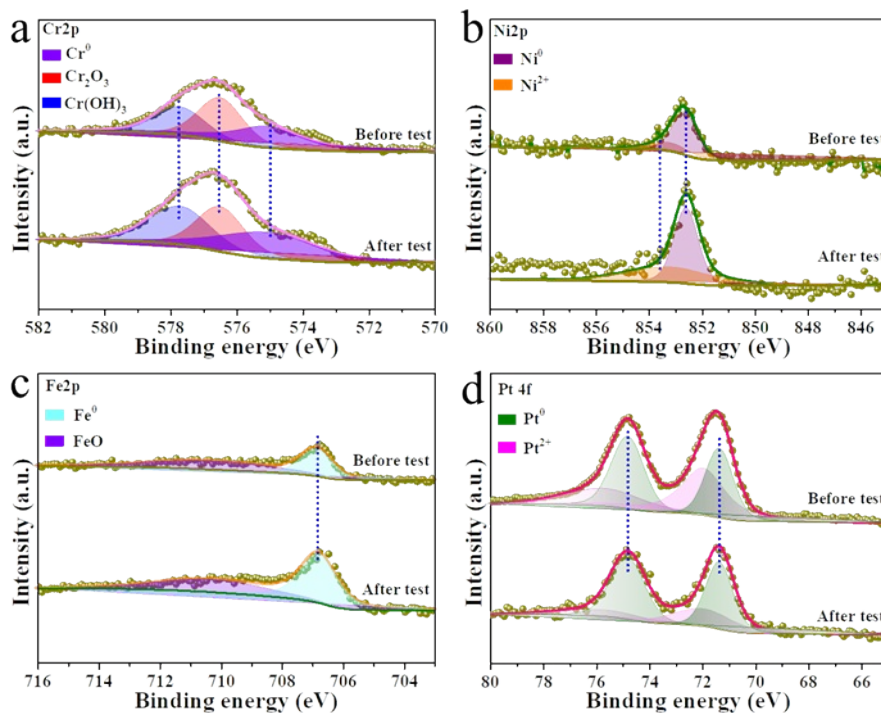


Fig. S11 XPS spectra of Pt@SM before and after stability test: (a) Cr2p, (b) Ni2p, (c) Fe2p, and (d) Pt4f.

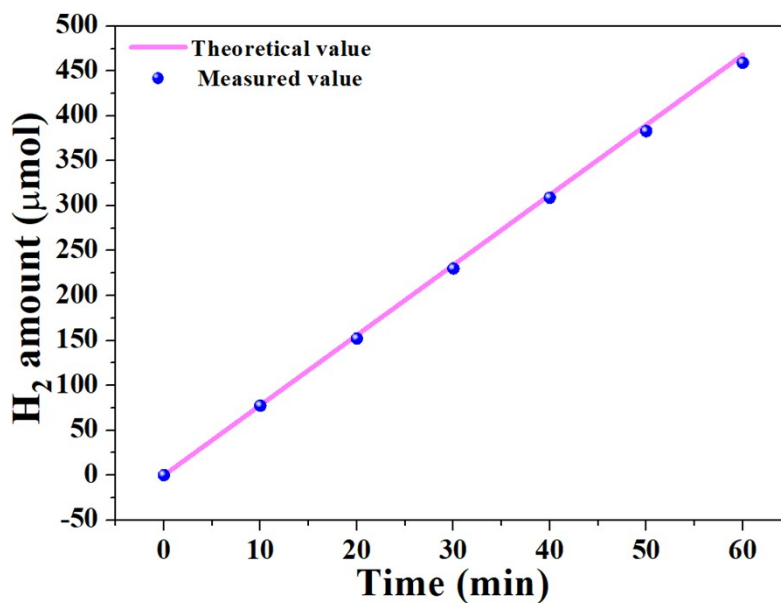


Fig. S12 H₂ amount evolved as a function of time at a constant current density of -50 mA cm⁻² over Pt@SM electrode.

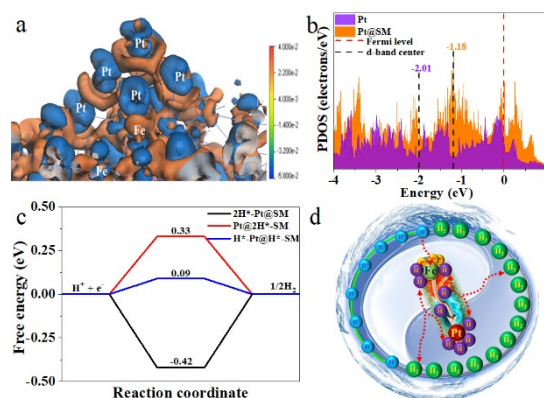


Fig. S13 (a) Charge density difference of Pt@SM, in which brown and blue indicates electron enrichment and depletion region, respectively. (b) PDOS of d orbitals for Pt atom on Pt (111) in Pt@SM and Pt (111). (c) ΔG_{H^*} on Pt atoms in Pt@SM, Fe atoms in Pt@SM, and Pt coupling with Fe atoms in Pt@SM. (d) Schematic illustration of the HER mechanism for Pt@SM.

As shown in **Fig. S14a**, the Pt nanoparticles are evenly deposited on carbon cloth. From the transmission electron microscopy image (**Fig. S14b**), the Pt nanoparticles are very small, and the average diameter of the Pt nanoparticles is similar to the Pt nanoparticles from Pt@SM. The high resolution transmission electron microscopy image of Pt@SM in **Fig. S14c** reveals that the distance of lattice fringes is about 0.224 nm, assigning to the (111) plane of cubic Pt (JCPDS#01-1194). It should be mentioned that the Pt content in Pt@CC from the ICP-OES result is about 0.12wt%, which is larger than that of Pt@SM, indicating that the Fe atoms in SM can enhance the HER performance of Pt nanoparticles through EMSI.

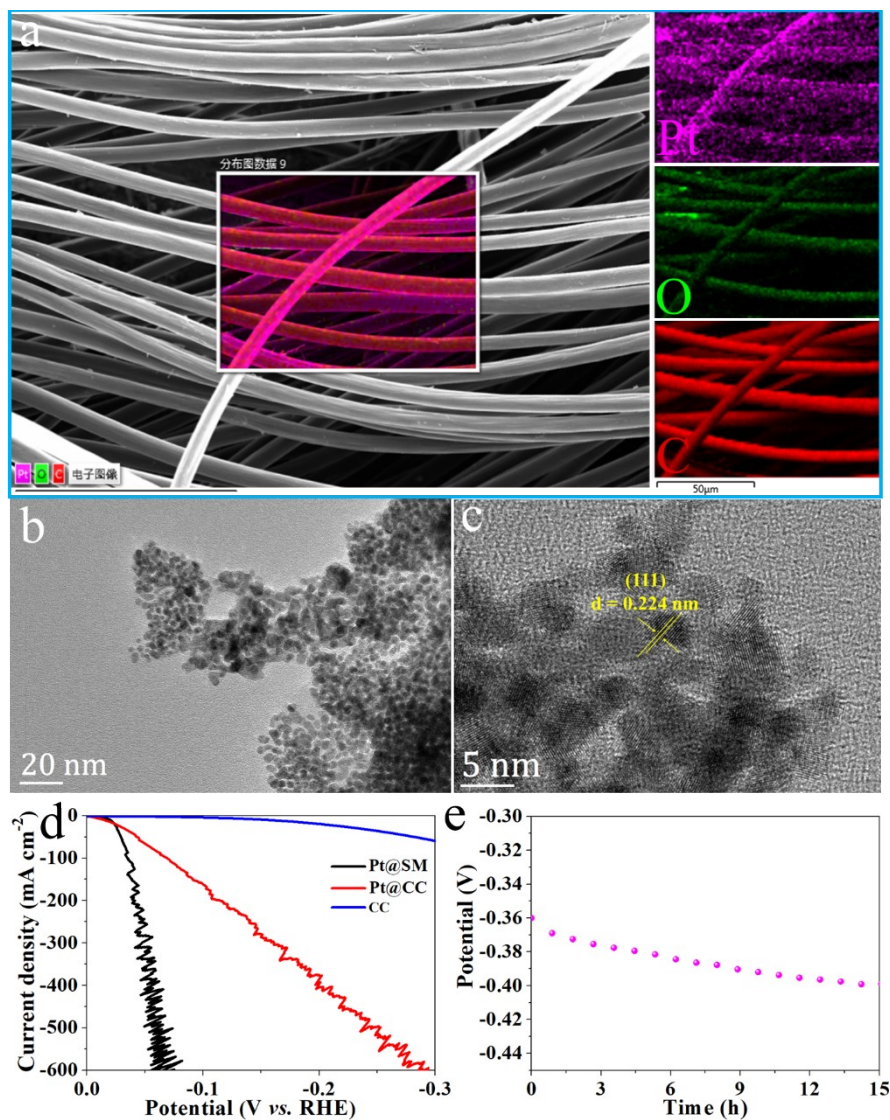


Fig. S14 (a) EDX mappings, (b) TEM, and (c) HRTEM images of Pt@CC. (d) LSV curves of Pt@SM, Pt@CC, and CC, (e) Time-dependent potential at -100 mA cm^{-2} without IR compensation for Pt@CC.

Table S1 Comparison of HER performance in acidic media for Pt@SM with other HER electrocatalysts at -100 mA cm^{-2} .

Catalysts	Overpotential (mV)	References
-----------	--------------------	------------

Pt@SM	34	This work
PtM@KB	55	8
Pt-Co/QNC-NH ₃	84	9
Pt/NC-850	152	10
Ir/C	64	11
Pt-DC	55	12
RPC@RPC	48	13
SS Pt-RuO ₂ HNSs	67	14
Ru _x Fe _y P-NCs/CNF	132	15
N-Co-S/G	125	16
Fe _{0.5} Co _{0.5} P/CC	98	17
Pt ₁ /NMC	55	18
Pt/GNs	44	19
CoS Ni P	88	20
Mo ₂ C	60	21
Mo ₂ C@NC@Pt	60	22

References

1. M. Ernzerhof and G. E. Scuseria, *J. Chem. Phys.*, 1999, **110**, 5029-5036.
2. G. Kresse and J. Furthmüller, *Comput. Mater. Sci.*, 1996, **6**, 15-50.
3. F. Zhuo, H. Qiao, J. Zhu, S. Wang, Y. Bai, X. Mao and H.-H. Wu, *Chinese Chem. Lett.*, 2021, **32**, 2097-2107.
4. J. P. Perdew, K. Burke and M. Ernzerhof, *Phys. Rev. Lett.*, 1996, **77**, 3865-3868.
5. G. Kresse and D. Joubert, *Phys. Rev. B*, 1999, **59**, 1758-1775.
6. H.-H. Wu, J. Zhu and T.-Y. Zhang, *Nano Energy*, 2015, **16**, 419-427.
7. W. He, R. Zhang, J. Zhang, F. Wang, Y. Li, J. Zhao, C. Chen, H. Liu and H. L. Xin, *J. Catal.*, 2022, **410**, 112-

120.

8. N. Nie, D. Zhang, Z. Wang, Y. Qin, X. Zhai, B. Yang, J. Lai and L. Wang, *Small*, 2021, **17**, 2102879.
9. J. Cheng, Z. Zhao, B. Zhang, J. Xu, C. Lin, X. Li and X. Gu, *J. Alloys Compd.*, 2022, **900**, 163441.
10. G. Jiang, C. Zhang, X. Liu, J. Bai, M. Xu, Q. Xu, Y. Li, L. Long, G. Zhang, S. Li and Y. He, *Int. J. Hydrogen Energy*, 2022, **47**, 6631-6637.
11. J. Hao, J. Hou, H. Wei, Z. Su, H. Li, L. Zhang and X. Gong, *Chem. Commun.*, 2022, **58**, 5606-5609.
12. W. Quan, X. Ruan, Y. Lin, J. Luo and Y. Huang, *Nanoscale*, 2021, **13**, 18677-18683.
13. J. Luo, J. Wang, Y. Guo, J. Zhu, H. Jin, Z. Zhang, D. Zhang, Y. Niu, S. Hou, J. Du, D. He, Y. Xiong, L. Chen, S. Mu and Y. Huang, *Appl. Catal., B*, 2022, **305**, 121043.
14. J. Wang, H. Yang, F. Li, L. Li, J. Wu, S. Liu, T. Cheng, Y. Xu, Q. Shao and X. Huang, *Sci. Adv.*, 2022, **8**, eabl9271.
15. B. Yang, J. Xu, D. Bin, J. Wang, J. Zhao, Y. Liu, B. Li, X. Fang, Y. Liu, L. Qiao, L. Liu and B. Liu, *Appl. Catal., B*, 2021, **283**, 119583.
16. P. Sabhapathy, I. Shown, A. Sabbah, P. Raghunath, J.-L. Chen, W.-F. Chen, M.-C. Lin, K.-H. Chen and L.-C. Chen, *Nano Energy*, 2021, **80**, 105544.
17. C. Tang, L. Gan, R. Zhang, W. Lu, X. Jiang, A. M. Asiri, X. Sun, J. Wang and L. Chen, *Nano Lett.*, 2016, **16**, 6617-6621.
18. H. Wei, H. Wu, K. Huang, B. Ge, J. Ma, J. Lang, D. Zu, M. Lei, Y. Yao, W. Guo and H. Wu, *Chem. Sci.*, 2019, **10**, 2830-2836.
19. X. Yan, H. Li, J. Sun, P. Liu, H. Zhang, B. Xu and J. Guo, *Carbon*, 2018, **137**, 405-410.
20. J. Sun, M. Ren, L. Yu, Z. Yang, L. Xie, F. Tian, Y. Yu, Z. Ren, S. Chen and H. Zhou, *Small*, 2019, **15**, e1804272.
21. G. Humagain, K. MacDougall, J. MacInnis, J. M. Lowe, R. H. Coridan, S. MacQuarrie and M. Dasog, *Adv. Energy Mater.*, 2018, **8**, 1801461.
22. J. Q. Chi, J. Y. Xie, W. W. Zhang, B. Dong, J. F. Qin, X. Y. Zhang, J. H. Lin, Y. M. Chai and C. G. Liu, *ACS Appl. Mater. Interfaces*, 2019, **11**, 4047-4056.